LETTER

https://doi.org/10.1038/s41586-018-0838-z

The surprisingly large neutron capture cross-section of ^{88}Zr

Jennifer A. Shusterman[1,2,3]*, Nicholas D. Scielzo[1], Keenan J. Thomas[1], Eric B. Norman[4], Suzanne E. Lapi[5], C. Shaun Loveless[5], Nickie J. Peters[6], J. David Robertson[6], Dawn A. Shaughnessy[1] & Anton P. Tonchev[1]

The probability that a nucleus will absorb a neutron—the neutron capture cross-section—is important to many areas of nuclear science, including stellar nucleosynthesis, reactor performance, nuclear medicine and defence applications. Although neutron capture cross-sections have been measured for most stable nuclei, fewer results exist for radioactive isotopes, and statistical-model predictions typically have large uncertainties[1]. There are almost no nuclear data for neutron-induced reactions of the radioactive nucleus ^{88}Zr, despite its importance as a diagnostic for nuclear security. Here, by exposing ^{88}Zr to the intense neutron flux of a nuclear reactor, we determine that ^{88}Zr has a thermal neutron capture cross-section of 861,000 ± 69,000 barns (1σ uncertainty), which is five orders of magnitude larger than the theoretically predicted value of 10 barns[2]. This is the second-largest thermal neutron capture cross-section ever measured and no other cross-section of comparable size has been discovered in the past 70 years. The only other nuclei known to have values greater than 10^5 barns[3–6] are ^{135}Xe (2.6×10^6 barns), a fission product that was first discovered as a poison in early reactors[7,8], and ^{157}Gd (2.5×10^5 barns), which is used as a detector material[9,10], a burnable reactor poison[11] and a potential medical neutron capture therapy agent[12]. In the case of ^{88}Zr neutron capture, both the target and the product (^{89}Zr) nuclei are radioactive and emit intense γ-rays upon decay, allowing sensitive detection of miniscule quantities of these radionuclides. This result suggests that as additional measurements with radioactive isotopes become feasible with the operation of new nuclear-science facilities, further surprises may be uncovered, with far-reaching implications for our understanding of neutron capture reactions.

The neutron capture reaction cross-sections for the vast majority of radioactive nuclei are poorly known, despite the importance of this information to a range of topics in both fundamental and applied nuclear science. Essentially all the elements that are heavier than iron were created via successive neutron capture reactions and β decays (which convert neutrons to protons within the nucleus) in celestial environments, such as asymptotic giant branch stars[13], core-collapse supernovae and neutron star mergers[14]. Understanding the origin of the elements in the cosmos is one of the most important overarching challenges in nuclear science and requires neutron capture cross-sections for radioactive nuclei produced along the nucleosynthesis pathways. Over the last century, nuclear reactors and weapons have exploited neutron-induced reactions to harness enormous amounts of energy, relying upon a detailed neutron inventory for predictable performance. In a nuclear reactor, nuclides with large neutron capture cross-sections act as poisons in the fuel and diminish performance, or can be introduced intentionally to control fuel reactivity. The United States' Science-Based Stockpile Stewardship Program, which is used to maintain high confidence in the safety, security, reliability and effectiveness of the nuclear stockpile in the absence of nuclear testing[15], relies in part on cross-sections for radioactive isotopes to interpret archival data from underground tests of nuclear devices. The transmutation of stable Y and Zr detector material used in underground tests produced radioactive isotopes, such as ^{88}Zr (half-life $t_{1/2} = 83.4$ d), that served as important diagnostics sensitive to neutron and charged-particle fluences[16]. However, nuclear reaction network calculations, which model the production and destruction of these radioactive isotopes, rely on cross-sections for which there are limited or no data, making it challenging to interpret the historical data. For ^{88}Zr, the only neutron (n) induced reaction that has been measured[17] is the ^{88}Zr(n,2n)^{87}Zr reaction at 14.8 MeV and there are no measurements of the ^{88}Zr(n,γ)^{89}Zr cross-section at any energy.

There are several challenges in performing neutron capture cross-section measurements on radioactive targets; these include the production, handling and purification of the target material, limitations on the neutron flux and the measurement timescale due to target or product half-life considerations, and the detection of the reaction channel amidst the radiation field produced by the target. Typically, with the small quantities of radioactive target atoms that can be collected, the highest-available neutron flux is required to transmute a large enough fraction of the target nuclei to make a measurement. For cases where the reaction product is radioactive, such as ^{89}Zr, activation measurements (where the reaction product can be identified after irradiation from its decay signature) are often the most sensitive. A measurement of the ^{88}Zr(n,γ)^{89}Zr reaction is ideally suited for the activation approach because ^{88}Zr β-decays with a 83.4-d half-life to ^{88}Y ($t_{1/2} = 106.626$ d), emitting a 392.87-keV γ-ray in 97.21% of the decays[18], whereas the reaction product ^{89}Zr β-decays with a 3.267-d half-life to stable ^{89}Y and emits a 909.15-keV γ-ray in 99.04% of the decays[19]. The fraction of the ^{88}Zr sample that is converted to ^{89}Zr can therefore be determined by detecting the characteristic γ-rays from the decays of these two isotopes following irradiation.

In this work, the ^{88}Zr(n,γ)^{89}Zr cross-section was measured by producing and chemically separating multiple ^{88}Zr samples, irradiating them in a high thermal-neutron flux of (6.7–8.7) $\times 10^{13}$ n cm^{-2} s^{-1} and determining the quantities of ^{88}Zr and of the reaction product ^{89}Zr using γ-ray spectroscopy. The ^{88}Zr target material was produced via the ^{89}Y(p,2n)^{88}Zr reaction using a proton (p) beam from the University of Alabama at Birmingham Cyclotron Facility. ^{88}Zr was chemically purified using anion-exchange chromatography and assayed before encapsulation as a salt residue in high-purity quartz tubes. The 37-kBq ^{88}Zr samples and accompanying quartz-encapsulated natural-metal foils (Fe, Zr, Mo and Y), which served as flux monitors, were irradiated for 5 min–50 h in a primarily thermal-neutron flux in the graphite reflector of the University of Missouri Research Reactor (MURR). The neutron flux was determined with precision of 7%–11% from reactions in the monitor foils (Extended Data Table 1), which have well established cross-sections[20], together with detailed MCNP5 (Monte Carlo N-Particle code, version 5) modelling of the neutron flux at the irradiation position to provide the neutron energy distribution (Extended Data Fig. 1).

Following irradiation, the ^{88}Zr targets were returned to Lawrence Livermore National Laboratory (LLNL) for γ-ray spectroscopy using

[1]Lawrence Livermore National Laboratory, Livermore, CA, USA. [2]Hunter College of the City University of New York, New York, NY, USA. [3]Graduate Center of the City University of New York, New York, NY, USA. [4]University of California, Berkeley, Berkeley, CA, USA. [5]University of Alabama at Birmingham, Birmingham, AL, USA. [6]University of Missouri, Columbia, Columbia, MO, USA. *e-mail: js7294@hunter.cuny.edu

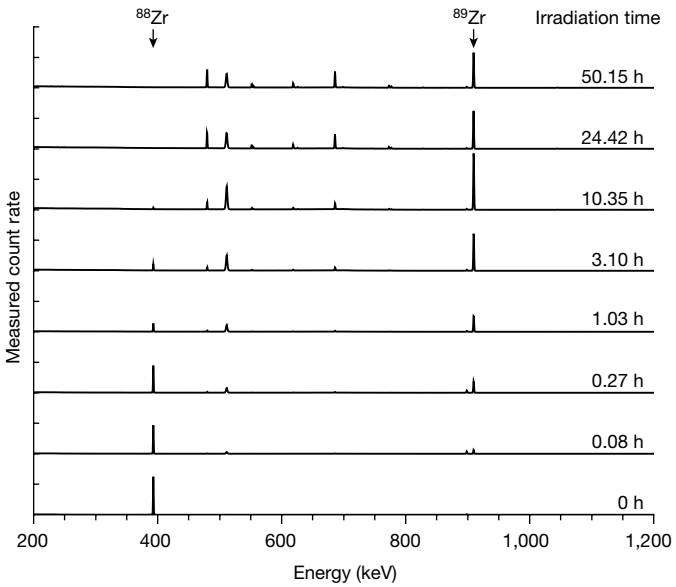

Fig. 1 | Representative γ-ray spectra from the irradiated ^{88}Zr samples. The spectra, which were collected with HPGe detectors immediately upon receipt at LLNL, are normalized on the basis of the live time of the measurement, initial target atoms and neutron flux. No decay or detector efficiency corrections have been applied. The unlabelled peaks between 400 and 800 keV, aside from the 511-keV peak, are from ^{187}W and ^{82}Br (activation products of residual impurities in the sample). The 511-keV pair-annihilation peak is primarily due to the positron emission from the decay of ^{89}Zr and follows a trend nearly identical to that of the 909-keV peak.

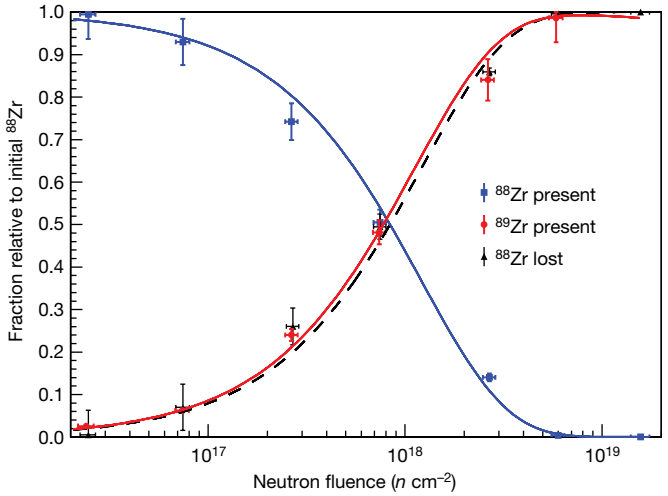

Fig. 2 | Populations of ^{88}Zr and ^{89}Zr as a function of neutron fluence. Measured ^{88}Zr atoms (blue squares) and ^{89}Zr atoms (red circles) present in the samples following irradiation, as well as ^{88}Zr atoms lost (black triangles), are normalized by the initial number of ^{88}Zr atoms in each sample. The blue solid, red solid and black dashed lines show the corresponding fitting curves. The Zr populations have been corrected for decay between the beginning of irradiation and the measurements performed after irradiation. The error bars (1σ uncertainties) represent the summed correlated and uncorrelated contributions.

high-purity germanium (HPGe) detectors. Counting of the irradiated samples started within two days of the end of bombardment (EOB) and continued over the course of several months to monitor the γ-rays emitted from the decays of ^{88}Zr, ^{89}Zr and ^{88}Y and to search for decay signatures of other species. As can be seen in Fig. 1, the ^{88}Zr activity decreased rapidly with irradiation time while the ^{89}Zr increased. Some variation between the spectra shown in Fig. 1 is due to differences in decay losses based on the length of irradiation and on when each sample was counted; in particular, the reduction in the 909-keV peak for the 24- and 50-h irradiations is primarily due to the decay of ^{89}Zr during irradiation. The identification of ^{89}Zr was unambiguous: all the γ-ray lines (at 909.15 keV, 1,620.8 keV, 1,657.3 keV, 1,713.0 keV and 1,744.5 keV) were detected (see Extended Data Fig. 2) and were observed to decay with an average half-life of 3.28 ± 0.05 d, which is in excellent agreement with the established ^{89}Zr half-life of 3.267 ± 0.005 d.

The number of atoms of each species was determined from these γ-ray peaks, after correcting for the ^{88}Zr and ^{89}Zr decay losses that occurred between the beginning of the irradiation and the γ-ray spectroscopy measurements. The measured quantities of ^{88}Zr and ^{89}Zr atoms present in each sample relative to the initial number of ^{88}Zr atoms are shown in Fig. 2. For each irradiation, the quantity of ^{89}Zr atoms present was consistent with the decrease observed in ^{88}Zr.

From these results, the thermal neutron capture cross-section for ^{88}Zr was determined to be (8.27 ± 0.64) × 10^5 b and (8.95 ± 0.72) × 10^5 b from independently analysing the burnup of ^{88}Zr and production of ^{89}Zr, respectively, where the 1σ uncertainties arise primarily from the determination of the neutron flux and the nuclear-decay counting. These values are in excellent agreement; averaging them gives the ^{88}Zr thermal neutron capture cross-section as $\sigma_{88} = (8.61 \pm 0.69) \times 10^5$ b, where the uncertainty is not reduced because the uncertainty contributions are largely common in the two analyses.

The ^{89}Zr(n,γ)^{90}Zr reaction, which has never been measured, was also included in the analysis and could affect the amount of ^{89}Zr observed, especially for the longer irradiations. However, because the data constrain the ^{89}Zr neutron capture cross-section to be less than 1.2 × 10^4 b, this reaction had negligible impact on the results.

A thorough assessment of potential competing reactions confirmed that no other mechanism contributed meaningfully to either the appearance of ^{89}Zr or disappearance of ^{88}Zr in the irradiated samples. ^{89}Zr could in principle be produced from traces of stable Y, Zr and Mo (approximately 0.3 ng, 90 ng and 5 ng, respectively) present in the samples, through the ^{89}Y(p,n)^{89}Zr, ^{90}Zr(n,2n)^{89}Zr and ^{92}Mo(n,α)^{89}Zr reactions, correspondingly. The γ-ray line for ^{89}Zr was small for natural Zr and absent for the Y and Mo irradiated monitor foils, indicating that these reactions contributed less than 10^{-5} in total to the ^{89}Zr inventory from the ^{88}Zr samples. Although at thermal energies (n,γ) cross-sections can become large owing to long neutron wavelengths, the transmutation of ^{88}Zr through competing (n,α) and (n,p) reactions is negligible because the emission of charged particles is highly suppressed by the limited penetrability of the nuclear Coulomb barrier. The self-attenuation of the neutron flux by the sample itself was estimated to be less than 0.003% using a ^{88}Zr thickness of about 4 × 10^{13} atoms per square centimetre, as determined from the minimum sample area, which was conservatively estimated to be 0.01 cm^2.

Because there are so few cross-sections of this magnitude known, consensus has not been reached in establishing an explanation that accounts for their behaviour[21]. Whereas ^{135}Xe, which has the largest known cross-section of 2.6 × 10^6 b, is one neutron away from the closed neutron shell at neutron number $N = 82$, and ^{88}Zr is two neutrons away from the closed neutron shell at $N = 50$, ^{157}Gd is not near a shell closure, and isotopes near shell closures do not seem to have enhanced cross-sections, as can be seen in Fig. 3[22–24]. Hussein et al.[21] discussed the statistical nature of very large neutron capture cross-sections and provided analysis supporting the random occurrence of doorway states interacting with compound-nucleus resonances that give rise to substantially enhanced reaction rates. The magnitude of the measured ^{88}Zr cross-section is particularly surprising because this nucleus has an even number of both protons and neutrons. The next largest value for a nucleus with these characteristics is 275 times smaller (^{196}Hg with 3,080 b) and such nuclei typically have lower thermal-neutron capture cross-sections than neighbouring isotopes with an odd number of either protons or neutrons. Existing predictions[2] indicate that the ^{88}Zr thermal neutron capture cross-section should be of the order of 10 b. No other known cross-section for a Zr isotope exceeds 1.2 b and no nucleus with fewer than 100 nucleons was previously known to have a cross-section

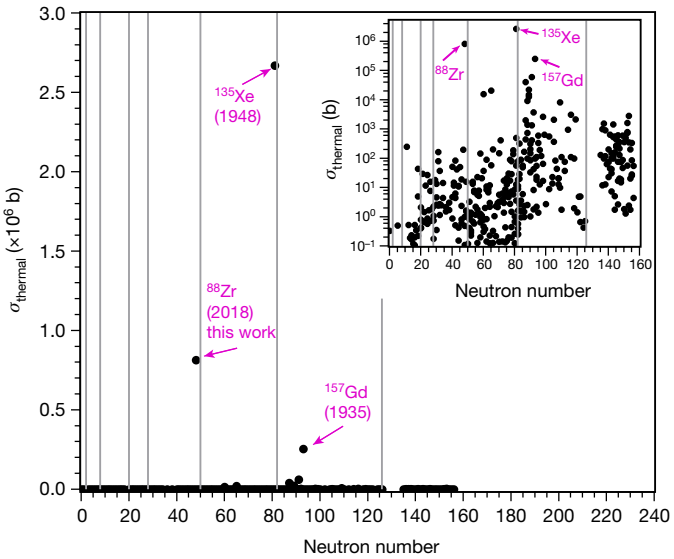

Fig. 3 | Measured thermal neutron capture cross-sections as a function of neutron number of the target. The main plot shows all the existing data on a linear scale, and the inset displays the same data on a logarithmic scale. The vertical lines indicate the neutron-shell closures, which occur for nuclei with 2, 8, 20, 28, 50, 82 and 126 neutrons. The three isotopes with cross-sections of more than 10^5 b are labelled along with the year of the measurement.

within a factor of 1,000 of this value (see Fig. 3). Although nuclei with such large neutron capture cross-sections appear to be rare, the two largest known values are both for radioactive isotopes, suggesting that additional examples may be found as experimental capabilities improve and measurements are performed with a broader range of radioactive nuclei and neutron energies.

Unprecedented quantities of radioactive isotopes are expected to be produced and collected at radioactive beam facilities, such as the Facility for Rare Isotope Beams (FRIB), which is anticipated to begin operations in the coming years. This will open up new opportunities to collect radionuclides in quantities suitable for targets[25], especially with the development of new isotope-harvesting techniques[26–28]. Additionally, new high-intensity neutron sources, such as the Frankfurt Neutron Source (FRANZ)[29] and the Soreq Applied Research Accelerator Facility (SARAF)[30], will increase the availability of intense neutron fluxes for measurements covering a wider range of neutron energies. Additional neutron reaction properties that defy expectations, such as this one, may be discovered and may prove to have important consequences for nucleosynthesis and for new applications of nuclear science.

Online content

Any methods, additional references, Nature Research reporting summaries, source data, statements of data availability and associated accession codes are available at https://doi.org/10.1038/s41586-018-0838-z.

Received: 5 May 2018; Accepted: 30 October 2018;
Published online 7 January 2019.

1. Bao, Z. Y. et al. Neutron cross sections for nucleosynthesis studies. *At. Data Nucl. Data Tables* **76**, 70–154 (2000).
2. Koning, A. J. & Rochman, D. Modern nuclear data evaluation with the TALYS code system. *Nucl. Data Sheets* **113**, 2841–2934 (2012).
3. Bernstein, S. et al. Neutron cross section of xenon-135 as a function of energy. *Phys. Rev.* **102**, 823–830 (1956).
4. Smith, E. C. et al. Total neutron cross section of Xe-135 as a function of energy. *Phys. Rev.* **115**, 1693–1699 (1959).
5. Dunning, J. R., Pegram, G. B., Fink, G. A. & Mitchell, D. Interaction of thermal neutrons with matter. *Phys. Rev.* **48**, 265–280 (1935).
6. Lapp, R. E., VanHorn, J. R. & Dempster, A. J. The neutron absorbing isotopes in gadolinium and samarium. *Phys. Rev.* **71**, 745–747 (1947).
7. Roggenkamp, P. L. The influence of Xenon-135 on reactor operations. In *Proc. 50 Years of Excellence in Science and Engineering at the Savannah River Site* 49–56 (US Department of Energy, 2000).
8. Watson, W. H. *The Poisoning of the NRX Pile.* Report No. TPI-51 AECL-732 (Atomic Energy of Canada, 1948).
9. Ovechkina, L., Riley, K., Miller, S., Bell, Z. & Nagarkar, V. Gadolinium loaded plastic scintillators for high efficiency neutron detection. *Phys. Procedia* **2**, 161–170 (2009).
10. Knoll, G. F. *Radiation Detection and Measurement* (John Wiley & Sons, Hoboken, 2010).
11. Galperin, A. Gd burnable poison system for reactivity control of the first cycle of a PWR. *Ann. Nucl. Energy* **14**, 53–57 (1987).
12. Shih, J. L. A. & Brugger, R. M. Gadolinium as a neutron-capture therapy agent. *Med. Phys.* **19**, 733–744 (1992).
13. Arlandini, C. et al. Neutron capture in low-mass asymptotic giant branch stars: cross sections and abundance signatures. *Astrophys. J.* **525**, 886–900 (1999).
14. Thielemann, F. K. et al. What are the astrophysical sites for the r-process and the production of heavy elements? *Prog. Part. Nucl. Phys.* **66**, 346–353 (2011).
15. Reis, V., Hanrahan, R. & Levedahl, K. The Big Science of stockpile stewardship. *Phys. Today* **69**, 46 (2016).
16. Hoffman, R. D., Kelley, K., Dietrich, F. S., Bauer, R. & Mustafa, M. *Modeled Neutron and Charged-Particle Induced Nuclear Reaction Cross Sections for Radiochemistry in the Region of Yttrium, Zirconium, Niobium, and Molybdenum*. Report No. UCRL-TR-222275 (Lawrence Livermore National Laboratory, 2006).
17. Prestwood, R. J., Thomas, K. W., Nethaway, D. R. & Smith, N. L. Measurement of 14-MeV neutron cross sections for ^{88}Zr and ^{88}Y. *Phys. Rev. C* **29**, 805–810 (1984).
18. McCutchan, E. A. & Sonzogni, A. A. Nuclear data sheets for A = 88. *Nucl. Data Sheets* **115**, 135–304 (2014).
19. Singh, B. Nuclear data sheets for A = 89. *Nucl. Data Sheets* **114**, 1–208 (2013).
20. Mughabghab, S. F. *Thermal Neutron Capture Cross Sections, Resonance Integrals and g-Factors.* Report INDC (NDS) 440 (International Atomic Energy Agency, 2003).
21. Hussein, M. S., Carlson, B. V. & Kerman, A. K. Statistical features of the thermal neutron capture cross sections. *Acta Phys. Pol. B* **47**, 391–405 (2016).
22. Ejnisman, R. et al. Neutron capture cross section of ^{44}Ti. *Phys. Rev. C* **58**, 2531–2537 (1998).
23. Beer, H. & Macklin, R. L. Measurement of the ^{85}Rb and ^{87}Rb capture cross sections for s-process studies. *Astrophys. J.* **339**, 962–977 (1989).
24. Singh, U. N. et al. Neutron resonance spectroscopy: chlorine. *Phys. Rev. C* **10**, 2138–2142 (1974).
25. Severin, G. W. Isotope harvesting at FRIB: additional opportunities for scientific discovery. Preprint at https://arxiv.org/abs/1812.03984 (2018).
26. Pen, A. et al. Design and construction of a water target system for harvesting radioisotopes at the National Superconducting Cyclotron Laboratory. *Nucl. Instr. Meth. Phys. Res. A* **747**, 62–68 (2014).
27. Mastren, T. et al. Harvesting ^{67}Cu from the collection of a secondary beam cocktail at the National Superconducting Cyclotron Laboratory. *Anal. Chem.* **87**, 10323–10329 (2015).
28. Schumann, D. & Neuhausen, J. Accelerator waste as a source for exotic radionuclides. *J. Phys. G* **35**, 014046 (2008).
29. Alzubaidi, S. et al. The Frankfurt neutron source FRANZ. *Eur. Phys. J. Plus* **131**, 124 (2016).
30. Tessler, M. et al. Neutron energy spectra and yields from the ^{7}Li(*p*,*n*) reaction for nuclear astrophysics. *J. Phys. Conf. Ser.* **665**, 012027 (2016).

Acknowledgements We thank N. Gharibyan, K. Moody, P. Grant, R. Henderson, G. Severin, G. Peaslee and M. Stoyer for discussions. We thank T. Wooddy for nuclear counting support and P. Spackman for inductively coupled plasma mass-spectrometry analysis. We also thank the operators and radiation safety staff of the University of Alabama at Birmingham Cyclotron for assistance in ^{88}Zr production and the irradiation services staff at MURR for experimental support at the reactor. This work was funded through LLNL LDRD 16-ERD-022 and was performed under the auspices of the US Department of Energy by LLNL under contract DE-AC52-07NA27344.

Reviewer information *Nature* thanks S. Heinitz, R. Rundberg and the other anonymous reviewer(s) for their contribution to the peer review of this work.

Author contributions J.A.S., N.D.S. and E.B.N. prepared most of the manuscript. J.A.S. performed the chemistry, target preparations, nuclear counting and data analysis. C.S.L. and S.E.L. performed the irradiation of the Y-sputtered Nb. N.J.P. carried out MCNP modelling. J.D.R. helped with the irradiation at MURR. K.J.T. did nuclear counting, reduction of γ-ray spectra and assisted with data analysis. J.A.S., E.B.N., N.D.S., K.J.T., A.P.T. and D.A.S. contributed to discussions on the results and interpretation of the data. All authors commented on the manuscript.

Competing interests The authors declare no competing interests.

Additional information
Extended data is available for this paper at https://doi.org/10.1038/s41586-018-0838-z.
Reprints and permissions information is available at http://www.nature.com/reprints.
Correspondence and requests for materials should be addressed to J.A.S.
Publisher's note: Springer Nature remains neutral with regard to jurisdictional claims in published maps and institutional affiliations.

METHODS

Production of ^{88}Zr. ^{88}Zr was produced from the ^{89}Y(p,2n) reaction using the TR24 cyclotron (Advanced Cyclotron Systems, Inc.) at the University of Alabama Cyclotron Facility. As described previously[31], high-purity monoisotopic yttrium was deposited by magnetron sputtering onto a 2.5-cm-diameter niobium disc. The niobium target and sputtered ^{89}Y (120–130 μm thick) were irradiated with 24-MeV protons for 60 min at 10 μA. After γ-ray analysis of the irradiated target, the measured EOB ^{88}Zr radioactivity was 3.96 MBq. Prior to chemical separation of the Zr, the irradiated target was allowed to decay for about 2.5 months so that the ^{89}Zr produced from the ^{89}Y(p,n) reactions would diminish by over six orders of magnitude; γ-ray spectroscopy performed after this decay period confirmed that the ratio of ^{89}Zr to ^{88}Zr atoms in the samples was less than 10^{-4}. The Y was then dissolved off the Nb disk using 4 M HCl, and this solution was evaporated to dryness and reconstituted in 37% HCl. Prior to loading on an anion-exchange column (AG1X8; 100–200 mesh, 0.6-cm-diameter and 7-cm-height resin bed), a couple of drops of 30% unstabilized H_2O_2 were added and the sample was heated briefly. The Y was eluted in concentrated HCl while the Zr was eluted in 2–4 M HCl. The Zr fractions (fraction volume 2 mL) were evaporated and redissolved in 37% HCl and the separation process was repeated. The final Zr fractions were concentrated to make a ^{88}Zr stock.

Target preparation. High-purity fused quartz (Suprasil 310, Heraeus) was used to encapsulate the ^{88}Zr residue as well as the monitor foils into separate sample and monitor tubes. The quartz was cleaned in an aqua regia bath, followed by thorough rinsing with Milli-Q water. The ^{88}Zr was deposited in the tubes after one end was sealed, and was allowed to evaporate to dryness before flame-sealing the other end under ambient conditions. The samples were leak-tested both at LLNL and MURR. The monitor foils were prepared and weighed before loading them into cleaned quartz tubes and sealing. For the three shorter irradiations, the flux monitors were Fe, Zr, Mo and Y. For the four longer irradiations, only Fe and Zr were used.

Target characterization. Each target contained 40.7–44.4 kBq of ^{88}Zr at the time of shipment to the reactor. The activity of each sample was determined to ±4% precision, limited by uncertainties in the nuclear counting geometry and location of ^{88}Zr within the samples. From the γ-ray spectrum of the original target (Extended Data Fig. 2a), it is evident that the dominant activity in the sample was ^{88}Zr, accompanied by some ^{88}Y produced primarily from the decay of ^{88}Zr. There was also a small amount of ^{56}Co, of the order of 10^8 atoms per target, which is an impurity produced from the Y target material. An aliquot of the final ^{88}Zr stock solution was evaporated and reconstituted in a solution of 2% HNO_3 and analysed using inductively coupled plasma mass spectrometry at the LLNL Forensic Science Center to determine the quantities of stable Zr, Y, Mo, Sr and Nb present in the sample. The resulting stable mass content for each of the irradiated samples could be determined by scaling these results using the ratio of the activity of each sample relative to the stock solution (as determined through γ-ray spectroscopy). From this information, the stable-element contents for each irradiated sample were determined to be in the ranges 0.65–0.74 ng for Sr, 0.27–0.31 ng for Y, 84.8–96.4 ng for Zr, 0.13–0.15 ng for Nb and 4.3–4.9 ng for Mo. The stable species present in the sample are from impurities in the original Y-sputtered coin target and reagents, not added carrier.

Irradiation. The targets and monitors were irradiated simultaneously in the graphite reflector at MURR. The irradiation times and sample contents are listed in Extended Data Table 2. After irradiation, the samples were removed from their cans in a hot cell, packaged and returned to LLNL.

Measuring samples after irradiation. At LLNL, the samples were unpacked and examined to verify that the integrity of the tubes was not compromised during irradiation. They were then washed in an aqua regia bath, followed by two Milli-Q water baths to remove external contamination from hot-cell processing at MURR. γ-ray spectroscopy was used to verify that none of the radionuclides of interest were detected in the aqua regia wash solutions. The samples were then counted using HPGe detectors at the Nuclear Counting Facility (NCF), in the same geometry used before irradiation. Counting began on most samples within 2 days of EOB. After the initial counts, the samples were opened and the interior of the tubes was washed with approximately 3 mL of 9 M HCl to dissolve the Zr residue. The decays of the dissolved samples and the quartz tubes were counted to determine the efficiency of removing the ^{88}Zr and ^{89}Zr from the tubes. In each case, more than 91% of the Zr was dissolved in the HCl—except for the 1-h and 50-h irradiations, for which 85% and 82% went into the HCl, respectively, with the remainder accounted for in the quartz tubes. The dissolved samples were diluted with Milli-Q water to 10 mL and counted in a standard counting geometry at the NCF. The monitor foils were removed from their quartz tubes and mounted on disks for counting. Each of the samples was counted on several detectors with relative efficiencies of 21%–37% (each calibrated for point-source samples to 1% fractional precision at the 1σ confidence level for use in GAMANAL[32] detector characterization), and the distance was adjusted to maintain a dead time of less than 15%. Just as with the initial activity determination, the ^{88}Zr and ^{89}Zr activities for each sample were determined to ±4% precision. Therefore, the ratio of activity present after irradiation to the initial ^{88}Zr activity before irradiation could be determined to be just under 6%. Aside from the 1% contribution from the point-source calibration of the HPGe detector efficiencies, which is correlated across all the measurements, the uncertainty arising from the spatial distribution and location was deemed to be uncorrelated from sample to sample. To verify that the γ-ray peaks decayed with the appropriate half-life for the isotope of interest, samples were counted over the course of several months at a constant distance (between 8 and 33 cm) on a 37% p-type coaxial detector.

Flux determination. The materials listed in Extended Data Table 1 were encapsulated in quartz tubes and irradiated alongside the ^{88}Zr samples to serve as flux monitors. The reactor fluxes at thermal ($E_n < 0.5$ eV) and resonance-region (0.5 eV $< E_n <$ 10 keV) neutron energies were determined from neutron capture reactions which produce ^{99}Mo, ^{95}Zr, ^{97}Zr, and ^{59}Fe from the Mo, Zr, and Fe samples using cross-sections from the International Atomic Energy Agency International Nuclear Data Committee[20]. The activities of these reaction products were determined through γ-ray spectroscopy using the same set of NCF detectors.

For a pair of reactions, for example ^{94}Zr(n,γ)^{95}Zr and ^{58}Fe(n,γ)^{59}Fe, the thermal and resonance flux contributions, Φ_t and Φ_r, respectively, were determined from the system of equations:

$$A_{95} = N_{94}(\sigma_{94,t}\Phi_t + \sigma_{94,r}\Phi_r)(1 - e^{-\lambda_{95}t_i})e^{-\lambda_{95}t_d}$$

$$A_{59} = N_{58}(\sigma_{58,t}\Phi_t + \sigma_{58,r}\Phi_r)(1 - e^{-\lambda_{59}t_i})e^{-\lambda_{59}t_d}$$

where A_{95} is the activity of ^{95}Zr determined from γ-ray spectroscopy, λ_{95} is the decay constant of ^{95}Zr, N_{94} is the number of ^{94}Zr atoms in the sample, t_i is the irradiation time, t_d is the time between EOB and counting, and $\sigma_{94,t}$ and $\sigma_{94,r}$ are the thermal and resonance-region cross-sections for the ^{94}Zr(n,γ)^{95}Zr reaction (with analogous notation for the ^{59}Fe quantities). The results from the available radionuclide pairs gave consistent values for the thermal and resonance region fluxes for each irradiation and were averaged to give the fluxes presented in Extended Data Table 1. The uncertainties in the neutron fluxes are 7%–11% and arise from a combination of uncorrelated terms (counting statistics, mass and irradiation times for each of the flux-monitor materials) and systematic uncertainties of 7% in the reference cross-section data, which were common across all samples.

Data analysis. The count rates of the γ-ray peaks at 393 keV and 909 keV from the various measurements were used to determine the activities of ^{88}Zr and ^{89}Zr, respectively, present in the samples at the time of the HPGe measurements. The corrections applied to account for the decay of ^{88}Zr and ^{89}Zr over the course of the experiment consisted of two parts: the decay during the irradiation and the decay between the EOB and the end of the HPGe measurement. For both the ^{88}Zr and the ^{89}Zr results, the decay between the EOB and the HPGe measurement followed simple first-order kinetics.

For ^{88}Zr, the corrections for decay during irradiation are <2% and straightforward to make because the timescales are much shorter than its 83.4-d radioactive half-life. The decay-corrected ^{88}Zr results, relative to the initial number of atoms of ^{88}Zr present in each sample, are shown in Fig. 2 with the total uncertainties arising from the determination of the activities and neutron fluxes described earlier (summarized in Extended Data Table 3).

The ^{88}Zr thermal neutron cross-section, σ_{88} (in units of square centimetres, converted to barns by 1 b = 10^{-24} cm^2), was determined from the samples by fitting the decay-corrected number of atoms of ^{88}Zr at the EOB, $N_{88}(\Phi)$, normalized by the initial number of ^{88}Zr atoms in each target, $N_{88}(0)$, using the relation:

$$\frac{N_{88}(\Phi)}{N_{88}(0)} = e^{-\Phi\sigma_{88}} \quad (1)$$

where Φ is the thermal neutron fluence in neutrons per square centimetre.

The result is $\sigma_{88} = (8.27 \pm 0.64) \times 10^5$ b when accounting for the correlated and uncorrelated contributions to the uncertainty in the atom ratios and fluence determinations for the data points. The fitting was performed using only the uncorrelated contributions (which yielded a total uncertainty of 3% when all seven measurements were considered together), and the correlated uncertainties (totalling just over 7%) were subsequently added in quadrature to the resulting fit uncertainty. For the atom ratios, the uncorrelated contributions were dominated by the uncertainty in the counting geometry due to the location of the activity within the tube, whereas for the neutron fluences they arose primarily from counting statistics and uncertainties in the masses and irradiation times of the monitor foils. The correlated uncertainties for the atom ratios were from the uncertainty in the photopeak efficiency of the HPGe detectors for well defined sample geometries, and those for the neutron fluences were dominated by the uncertainties in the reference cross-sections. Additional contributions from decay data were considerably smaller than the uncertainties arising from the reference cross-sections. The fraction of ^{88}Zr lost to burnup in each sample is also shown in Fig. 2 and was determined as $1 - N_{88}(\Phi)/N_{88}(0)$.

An additional value for σ_{88} was obtained by analysing the appearance of ^{89}Zr atoms in the irradiated samples. The interpretation of the ^{89}Zr data also required applying decay corrections, but in this case these corrections are a little more complicated. The decay during irradiation depends on the rate of ^{89}Zr production which, in turn, depends on both the neutron flux (which varied from sample to sample) and the ^{88}Zr thermal neutron capture cross-section. However, the ^{89}Zr was observed to be produced on a timescale substantially shorter than the radioactive half-life of ^{89}Zr, and therefore the correction is relatively insensitive to the exact value of the ^{88}Zr thermal-neutron capture cross-section. The cross-section measured from the ^{88}Zr data was used as an initial value to calculate the production rate of ^{89}Zr and therefore the decay correction. For irradiations shorter than 3 h the correction is less than 2% and grows to be about 34% for the longest irradiation. Varying the cross-section and flux across the full range of 1σ uncertainty for the longest irradiation results in less than 1% variation in the total decay-corrected number of ^{89}Zr atoms produced.

An additional correction, applied to determine the number of ^{89}Zr nuclei produced, adjusts for the fact that not every neutron capture by ^{88}Zr ultimately yields ^{89}Zr in the ground state. ^{88}Zr, which has a nuclear spin-parity of 0^+, preferentially populates $1/2^+$ states in ^{89}Zr just above the neutron separation energy through *s*-wave neutron capture. The subsequent de-excitation through γ-ray emission populates the spin-$1/2^-$ ^{89}Zr isomer above the ground state, which has a spin-parity of $9/2^+$. The isomer decays with a branching ratio of 93.77% to the ^{89}Zr ground state; the remainder undergoes electron-capture decay to ^{89}Y and does not emit 909-keV γ-rays. Therefore, the ^{89}Zr population determined from the ground-state decays was divided by this branching ratio to determine the total number of ^{89}Zr atoms produced from the neutron capture reaction.

The determination of σ_{88} from these decay-corrected ^{89}Zr data as a function of neutron fluence must take into account not only the production of ^{89}Zr from ^{88}Zr but also the potential loss of ^{89}Zr due to additional neutron capture to form ^{90}Zr. The number of ^{89}Zr atoms produced during the irradiation, $N_{89}(\Phi)$, therefore depends on both the thermal neutron cross-sections of ^{88}Zr and ^{89}Zr through the following relation:

$$N_{89}(\Phi) = N_{88}(0)\frac{\sigma_{88}}{\sigma_{89} - \sigma_{88}}(e^{-\Phi\sigma_{88}} - e^{-\Phi\sigma_{89}}) \quad (2)$$

where the ^{89}Zr thermal neutron cross-section is denoted as σ_{89}. The data shown in Fig. 2 give $\sigma_{88} = (8.95 \pm 0.72) \times 10^5$ b and constrains σ_{89} to be less than 1.2×10^4 b, where the uncertainties were handled in the same way as for the previous fit.

The cross-sections determined from the ^{88}Zr and ^{89}Zr data were averaged to determine the ^{88}Zr neutron capture cross-section; this yields $\sigma_{88} = (8.61 \pm 0.69) \times 10^5$ b with a fractional uncertainty that is not reduced because it arises from essentially identical sources in the two measurements.

Data availability

The data supporting the findings of this study are presented within this Letter and its Extended Data.

31. Queern, S. L. et al. Production of Zr-89 using sputtered yttrium coin targets. *Nucl. Med. Biol.* **50**, 11–16 (2017).
32. Gunnink, R. *Computerized Quantitative Analysis of Gamma-Ray Spectrometry.* Report No. UCRL-51061 (Lawrence Livermore Laboratory, 1972).

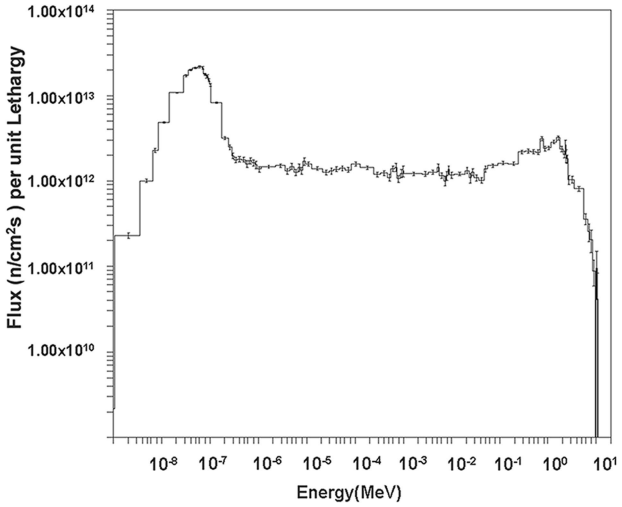

Extended Data Fig. 1 | Neutron energy spectrum calculated using MCNP5. The spectrum corresponds to the location where the samples were irradiated in the graphite reflector at MURR (position G1). The average thermal and resonance-region neutron fluxes were measured to be 7.1×10^{13} *n* cm^{-2} s^{-1} and 2.7×10^{12} *n* cm^{-2} s^{-1}, respectively. The flux of neutrons with energies above 12.5 MeV was determined using the monitor reaction $^{90}Zr(n,2n)^{89}Zr$ to be 4.5×10^{9} *n* cm^{-2} s^{-1}.

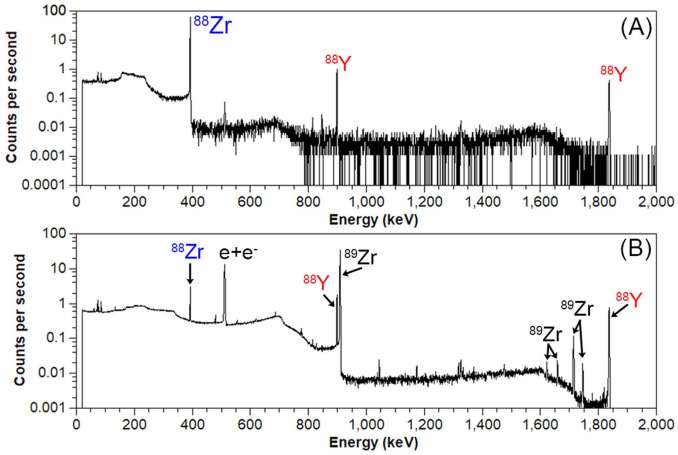

Extended Data Fig. 2 | Example γ-ray spectra for a ^{88}Zr sample, collected before and after neutron irradiation. a, Prior to irradiation, the γ-ray spectrum is dominated by the 393-keV line from the decay of ^{88}Zr accompanied by its daughter, ^{88}Y, which is formed between stock preparation and target encapsulation. **b**, The same sample, counted seven days after the 10.35-h irradiation at MURR, after dissolution. Following irradiation, there is a considerable amount of ^{89}Zr present, whereas the ^{88}Zr activity has decreased, indicating conversion of ^{88}Zr to ^{89}Zr. The other small γ-ray lines in **a** are from ^{56}Co impurities and in **b** are from activation products (^{82}Br and ^{187}W) of impurities present in the sample.

Extended Data Table 1 | Measured neutron flux in the thermal and resonance regions

Sample	Measured Average Flux (n/cm^2/s) Thermal (×10^{13})	Resonance (×10^{12})	Ratio Thermal/Resonance	Monitor Foils Used
1	8.54±0.77	2.74±0.41	31.17	Fe, Zr, Mo, Y
2	7.65±0.61	2.35±0.34	32.59	Fe, Zr, Mo, Y
3	7.30±0.52	2.43±0.33	30.05	Fe, Zr, Mo, Y
4	6.68±0.48	2.79±0.37	23.92	Fe, Zr
5	7.20±0.52	2.59±0.34	27.80	Fe, Zr
6	6.81±0.52	2.60±0.35	26.23	Fe, Zr
7	8.71±0.96	4.23±0.71	20.59	Fe, Zr

The listed data are based on measurements with the Zr, Fe and Mo flux monitors. Each of the monitors listed was irradiated along with the ^{88}Zr sample. For the first three monitors, six neutron capture reactions with known cross-sections were used to determine the average flux, whereas for the last four monitors three reactions were used.

Extended Data Table 2 | Activities before and after irradiation

Sample	^{88}Zr activity at beginning of irradiation (kBq)	Irradiation time (hrs)	^{88}Zr activity at EOB (kBq)	^{89}Zr activity at EOB (kBq)
1	37.0 ± 1.5	0.08	36.8 ± 1.5	19.1 ± 0.8
2	37.5 ± 1.5	0.27	34.9 ± 1.4	55.4 ± 2.4
3	34.9 ± 1.4	1.03	25.8 ± 1.1	194.2 ± 8.0
4	35.3 ± 1.4	3.10	17.8 ± 0.8	400.5 ± 16.4
5	36.0 ± 1.4	10.35	5.1 ± 0.3	679.3 ± 27.7
6	33.2 ± 1.3	24.42	0.13 ± 0.02	659.1 ± 26.9
7	35.8 ± 1.4	50.15	< 0.003	568.3 ± 23.6

The ^{88}Zr and ^{89}Zr activities are decay-corrected back to the EOB, but not corrected for decay during irradiation. The ^{89}Zr activities are for the ground state only and therefore not corrected for the decay branching ratio from the isomer to the ground state. For sample 7, no ^{88}Zr was detected, so an upper limit is presented.

Extended Data Table 3 | Summary of uncertainties

Source of Uncertainty	Magnitude	Correlated/Uncorrelated
Neutron Fluence		
Monitor mass	0.2-11%	Uncorrelated
Irradiation time	0.02-10%	Uncorrelated
Point-source calibration of HPGe efficiency	1%	Correlated
Counting statistics	<2%	Uncorrelated
Reference cross-section data	7%	Correlated
Final-to-intial atom ratios		
Sample geometry	6%	Uncorrelated
Point-source calibration of HPGe efficiency	1%	Correlated
Counting statistics	1-9%	Uncorrelated

The neutron capture cross-section was determined from the dependence of the final-to-initial atom ratios on the neutron fluence. The uncertainty contributions to these quantities are shown and are identified as correlated or uncorrelated for the seven measurements. The data were fitted using the uncorrelated contributions; the resulting total uncorrelated uncertainty was added in quadrature to the correlated values, yielding a total uncertainty on the cross-section of 8%.